Image Registration for Quantitative Analysis of Kidney Function using MRI

Rosario Sance [*], María J. Ledesma-Carbayo [*], Arvid Lundervold [†] and Andrés Santos [*]

[*] *Biomedical Image Technologies, Universidad Politécnica de Madrid, Avda. Ciudad Universitaria s/n, 28040, Madrid, Spain*

[†] *Department of Biomedicine, University of Bergen, Jonas Lies vei 9, NO-5009, Bergen, Norway*

Abstract. The aim of the present study is to analyze the possibilities of registration algorithms to compensate respiratory motion and deformation in abdominal DCE-MRI 3D temporary series. The final objective is that from registered data, appropriate intensity curves of local renal activity along the time could be represented for each kidney voxel. Assuming a relation between the voxel intensity and the contrast media concentration, this non-invasive renographic method could be used to evaluate the local renal function, and to calculate typical renal parameters like *glomerular filtration rate.*

Keywords: Non-rigid registration, kidney, renal function, DCE-MRI.
PACS: 87.57.-s, 87.57.Gg, 87.61.-c.

INTRODUCTION

Renal function is usually measured on the basis of serum creatinine level, creatinine and inulin clearance rate or plasma analysis. However, these methods assess the total nephron population of both kidneys and also require collection of blood and urine samples [1]. Since image-based renographic methods are less invasive and can assess each kidney separately, even at different depths of the parenchyma, several approaches with different medical image modalities and contrast materials have been developed.

To the best of our knowledge, manual alignment, segmentation [2], 2D rigid registration [3] or breath-hold acquisitions with fast sequences [4] have been previously applied in order to deal with the kidney motion induced by respiration and pulsations. Recently, a very promising 4D renographic registration framework based on Fourier and Wavelet transforms has also been approached [5].

In this paper we propose an efficient and automated non-rigid registration algorithm to correct motion and deformation of the kidneys in 3D Dynamic Contrast Enhanced Magnetic Resonance Imaging (DCE-MRI) series, as suggested in [6].

CP860, *Information Optics: 5th International Workshop,*
edited by G. Cristóbal, B. Javidi, and S. Vallmitjana
© 2006 American Institute of Physics 978-0-7354-0356-7/06/$23.00

MATERIALS AND METHODS

Our research was carried out with Gd-DTPA enhanced 3D MRI series of the abdominal region in healthy volunteers. Since Gd quelate is a paramagnetic contrast agent which presents the property of being mainly eliminated in the glomerulus of the kidney, the evaluation of typical renal function parameters like *Glomerular Filtration Rate* (GFR) is expected from the tracking of this passage.

The non-rigid registration algorithm next introduced was evaluated on four data sets, acquired under the general characterization and parameters presented on **TABLE1.**

TABLE 1. Characterization of the DCE-MRI data sets registered.

Series Id.	Scanner	Sequence	Resolution (mm)	4D Size	Timing
1	1.5 T Siemens Symphony	FLASH	(1.48x1.48x3.00)	(256x256x20x20)	Not equidistant
2	1.5 T Siemens Symphony	VIBE	(1.48x1.48x3.00)	(256x256x20x118)	One frame every 2.5 sec.
3	3.0 T Signa Excite GE	LAVA	(1.37x1.37x4.00)	(256x256x12x64)	One frame every 3.0 sec.
4	3.0 T Signa Excite GE	LAVA	(0.86x0.86x1.20)	(512x512x44x60)	One frame every 3.0 sec.

Non-Rigid Registration Algorithm Description

A major challenge of the registration algorithm is related to the signal intensity changes induced by the tracer passage. For that reason our algorithm is similar to those used for multimodality registration.

In spite of previous works suggesting head-to-feet constraints or simply affine models to describe kidney motion, we considered that rigid approaches did not show accuracy enough for the deformation correction task, so we implemented our method by defining a non-rigid transformation based on a B-Splines field with a uniformly spaced grid of control points.

In a registration process, the metric evaluates the similarity criterion between the reference image voxels against the corresponding in the transformed test image. When a point is mapped from one space to another by the transform, it will in general be mapped to a non-grid position, and interpolation will be required to evaluate the metric on it. On the other hand, interpolations are executed thousands of times in a single optimization cycle and affect the smoothness of the optimization search space. Hence, the trade-off between the simplicity of computation and the smoothness of the optimization must be taken into account to choose the interpolation scheme. Considering the selected B-Spline transform, we decided to include a B-Spline interpolator.

Regarding to the metric, we relied on information theory by using mutual information as the metric for our method, since this statistic method is not modality

dependant and yields quite a good robustness. Moreover, we worked with the *Mattes* implementation [7], since it does not require preprocessing and uses fewer parameters than the *Viola&Wells* approach. For this implementation, the negative of the mutual information ***S*** between the reference and test images (1), expressed as a function of the transformation parameters, is the discrepancy measure to be minimized:

$$S(\mu) = -\sum_{\iota}\sum_{\kappa} p(\iota,\kappa|\mu)\log\frac{p(\iota,\kappa|\mu)}{p_T(\iota|\mu)p_R(\kappa)} \tag{1}$$

where p, p_T and p_R are the joint, marginal test and marginal reference probability distributions, respectively.

In order to steer the improvement of the metric value, we chose a quasi-Newton optimizer, *BFGS*, because it provides superlinear convergence, and does not require second derivatives. In this particular case, a limited memory implementation was included [8], which only stores the last Hessian approximations instead of the whole history, and is strongly recommended for solving large non-linear optimization problems with simple bounds. A quadratic model (2) of the function value f is formed at every iteration x_k:

$$m_k(x) = f(x_k) + g_k^T(x - x_k) + \frac{1}{2}(x - x_k)^T B_k(x - x_k) \tag{2}$$

At every iteration x_k the algorithm stores only a small number m, of correction pairs $\{s_i, y_i\}, i = k-1,...,k-m$ (3),

$$s_k = x_{k+1} - x_k,\ y_k = g_{k+1} - g_k \tag{3}$$

containing information about the curvature of the function, and defining the limited memory iteration matrix B_x.

Finally, to reduce the computational time and increase the robustness of the algorithm, we used a multiresolution strategy based on the *Kybic* approach [9], in which the upsampling is applied alternatively on the input images and on the deformation model. At the same time, other parameters of the metric and the optimizer were changed, also contributing to create a coarse-to-fine effect.

The registration was yielded by referring all the frames in every series to a single one, usually the first on time. Attempts to chain every frame to the previous in time incremented the accumulated error without providing any other remarkable improvement, so this procedure was ruled out.

Neither pre-processing nor post-processing were applied to the data series.

FIGURE 1 shows the global scheme of the registration algorithm, which was implemented using the open source software toolkit for segmentation and registration of medical images, *ITK* (*Insight Toolkit*)[§].

[§] ITK, www.itk.org.

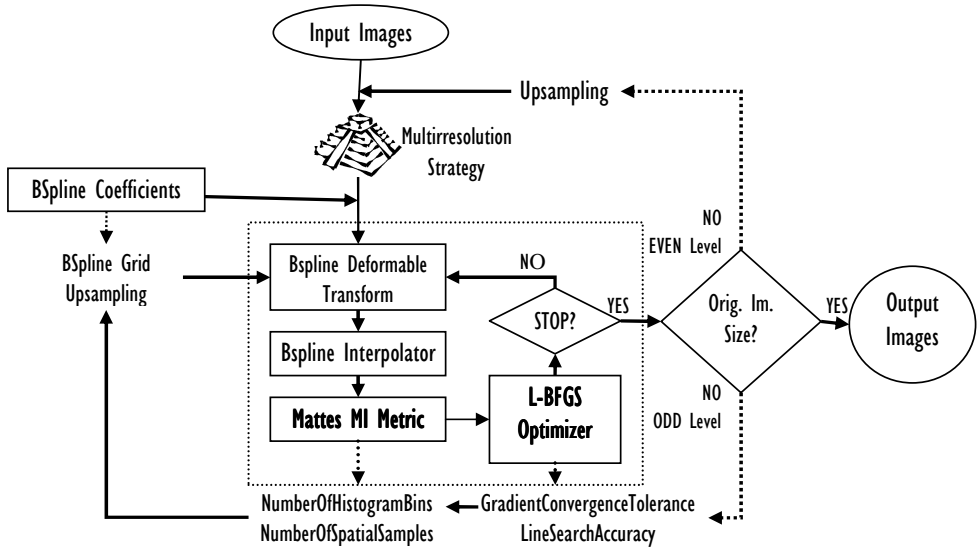

FIGURE 1. Global schematic diagram of the implemented non-rigid registration algorithm.

Pharmacokinetic multi-compartment modeling

We assumed the multi-compartment model proposed by *Lee* [10] to represent the pharmacokinetics of Gd-DTPA in every kidney region during time (**FIGURE 2**). It is a simple model even though the real kidney vasculature is quite more complex, but it seems to be enough for our requirements.

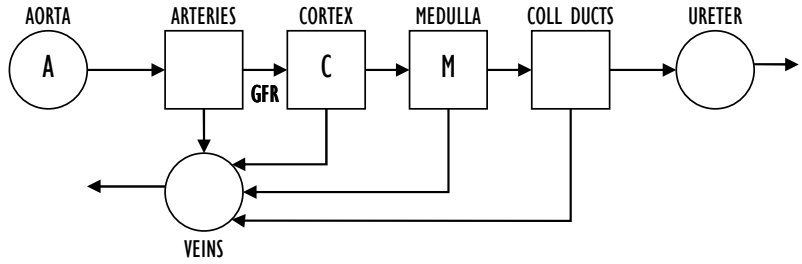

FIGURE 2. Kidney multi-compartment model proposed by *Lee et al.* for the Gd-tracer pharmacokinetics.

The presented model assumes that the tracer (Gd quelate) is confined to the plasma volume of the blood pool and to the intratubular volume within the nephron. Based on the pictured model, a set of ordinary differential equations was derived to predict the contrast agent concentration in each compartment. The respective coefficients of the

differential equations were calculated based on estimates of compartment volumes and flow rates found in the literature, and on individually measured GFR values. From the known input function, predicted time-concentration curves for every compartment were computed, which we used as a reference or sample to evaluate our results.

Therefore on our registered series, by defining anatomical regions of interest (ROIs) for aorta, renal arteries, renal cortex and medulla, time-intensity curves were plotted for every ROI and compared with the expected profiles. The advantage of working with ROIs instead of individual voxels is that the averaging minimizes the effect of the noise (statistical error, scatter, artifacts,...).

RESULTS

We have represented the outcome of the registration method applied to the 3D DCE-MRI series by means of composite slice images (**FIGURE 3**). These "checker-board" images show parts of the reference image and parts of the resampled test image in order to depict the continuity of contours before and after the alignment. The orange circles emphasize the most relevant changes and remarkable improvements.

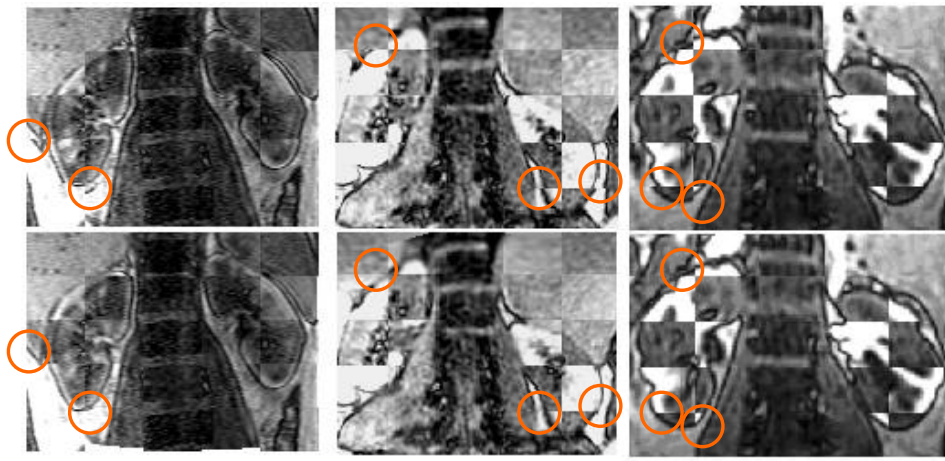

FIGURE 3. Registration results. Composite images before (*upper*) and after (*lower*) alignment. Slices extracted from one of the 1.5 T (*left*) and both of the 3T (*middle* and *right*) DCE-MRI series.

To create the resampled frame, the last saved transform from the finest level of the multirresolution pyramid is applied to the correspondent test image. Since the most evident kidney motion is produced on the coronal plane, the deformation field applied to compensate the breathing motion presents a tendency spread over it, as shown in **FIGURE 4**.

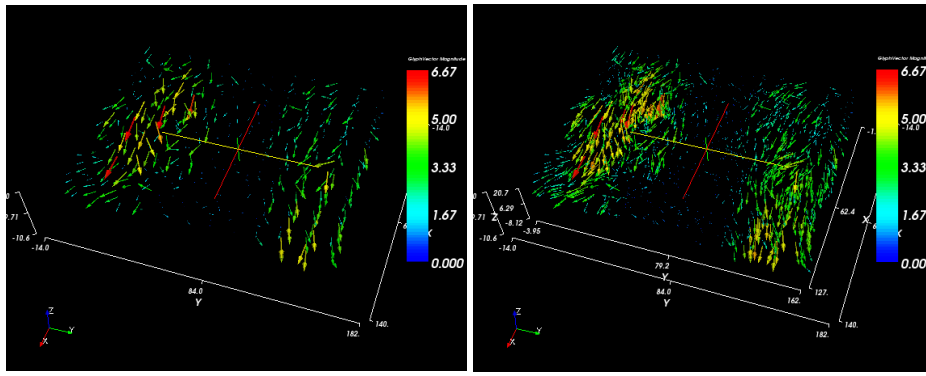

FIGURE 4. Registration of two frames belonging to the first 1.5T DCE-MRI series. *Left*: Final transform for the control points of the B-Splines grid. *Right*: Deformation field comprising every voxel in the image.

DISCUSSION

Three-dimensional DCE-MR renography with motion correction enables voxel-wise determination of tracer concentration versus time by considering the voxels intensity evolution. In this way, the local renal function can be estimated from time courses in selected ROIs (**FIGURE 5**).

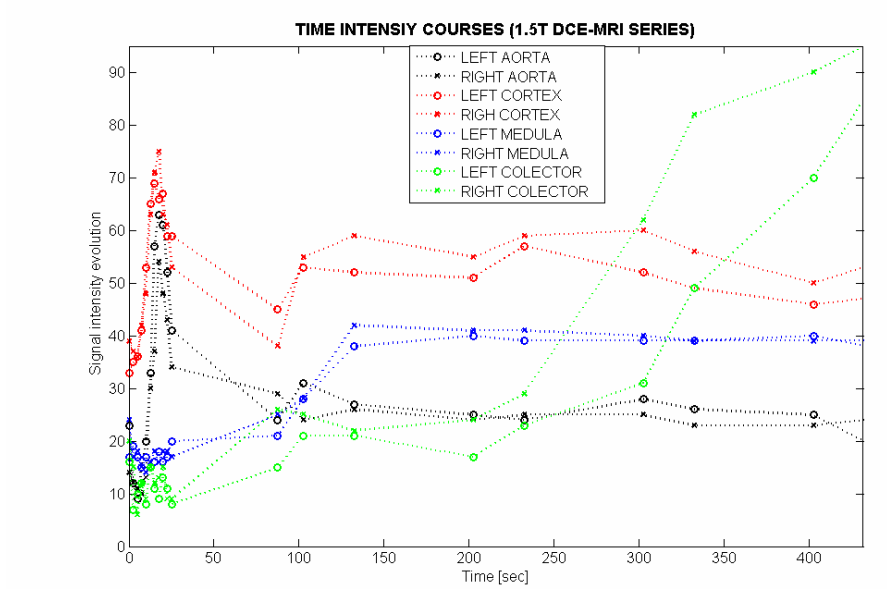

FIGURE 5. Estimation of the Gd-concentration versus time approximated by the signal intensity evolution. Typical renal profiles for the anatomical regions selected on a slice belonging to the first 1.5T DCE-MRI series.

The real relationship between the signal intensity evolution and the tracer concentration is non-linear and highly dependent on some acquisition parameters like the intrinsic tissue *T1* value [11], so actually it is given by means of a calibration curve.

The proposed elastic registration algorithm, correcting the geometric displacements of the kidney during data collection, will therefore allow local and more accurate estimation of kidney function, with potential impact on diagnosis and follow-up in patients with kidney disease.

ACKNOWLEDGMENTS

The authors would like to thank Jarle Rorvik and the Department of Radiology of the University of Bergen for providing the DCE-MRI data series to carry out this study.

Partial founding from EC COST B21 is acknowledged.

REFERENCES

1. N. Grenier, F. Basseau, M. Ries et al., Abdom Imaging **28** (2), 164 (2003).
2. V. S. Lee, H. Rusinek, M. E. Noz et al., Radiology **227** (1), 289 (2003).
3. Y. Sun, M. P. Jolly, and J. M. F. Moura, Medical Image Computing and Computer-Assisted Intervention - Miccai 2004, Pt 1, Proceedings **3216**, 903 (2004).
4. P. V. Prasad and A. Priatna, Eur J Radiol **29** (2), 133 (1999).
5. T. Song, V. S. Lee, H. Rusinek et al., Int Conf Med Image Comput Assist Interv **8** (Pt 2), 205 (2005).
6. N. Michoux, X. Montet, A. Pechere et al., Eur J Radiol **54** (1), 124 (2005).
7. D. Mattes, D. R. Haynor, H. Vesselle et al., Journal of Nuclear Medicine **42** (5), 11P (2001).
8. Dong C. Liu and Jorge Nocedal, Mathematical Programming **45** (1 - 3), 503 (1989).
9. J. Kybic, P. Thevenaz, A. Nirkko et al., IEEE Trans Med Imaging **19** (2), 80 (2000).
10. V. S. Lee, H. Rusinek et al., Proc. Intl. Soc. Mag. Reson. Med **9**, 2059 (2001).
11. P. Armitage, C. Behrenbruch, M. Brady et al., Medical Image Analysis **9** (4), 315 (2005).